Studies of the Chemical and Pore Structures of the Carbon Aerogels Synthesized by Gelation and Supercritical Drying in Isopropanol

Ruowen Fu,[1,2] Bo Zheng,[3] Jie Liu,[3] Steve Weiss,[1] Jackie Y. Ying,[1] Mildred S. Dresselhaus,[1] Gene Dresselhaus,[1] Joe Satcher, Jr.,[4] and Theodore Baumann[4]

[1]*Massachusetts Institute of Technology, 77 Massachusetts Avenue, Cambridge, Massachusetts 02139*
[2]*PCFM Laboratory, Zhongshan University, Guangzhou, 510275 China*
[3]*Department of Chemistry, Duke University, Durham, North Carolina 27708*
[4]*Lawrence Livermore National Laboratory, P.O. Box 808, Livermore, California 94551*

Received 11 April 2003; accepted 11 August 2003

ABSTRACT: The carbon aerogels prepared by a new method through gelation and supercritical drying in isopropanol were characterized by X-ray photoelectron spectroscopy (XPS), scanning electron microscopy, and a surface area analyzer. Their chemical structure, morphology, and pore structure are discussed. We found that all of these carbon aerogel (CA-IPA) samples have almost the same carbon and oxygen elemental states, as well as similar oxygen-containing groups. The curve fitting of the C1s XPS spectra of the samples for characterizing oxygen-containing surface groups can be performed by assuming the peak type to be a Gaussian–Lorentzian Cross Product, but we cannot obtain good results using a Gaussian lineshape. When the mass density of the CA-IPA decreases, the mesopores and macropores of the samples are found to grow, but the size and the shape of individual carbon nanoparticles in various CA-IPA samples do not apparently change. The micropore volume of the CA-IPA samples increases with a decrease in the mass density, while the mesopore volume has a maximum at a certain mass density. The CA-IPA samples have a very narrow micropore distribution at about 0.5 nm. The mesopore distribution of the CA-IPA is widened and the average pore size increases as the mass density of the sample decreases. © 2004 Wiley Periodicals, Inc. J Appl Polym Sci 91: 3060–3067, 2004

Key words: carbon aerogel; gelation and drying in isopropanol; chemical structure; pore structure

INTRODUCTION

The fabrication of carbon aerogels is an important subject both with regard to science and to applications. There are many papers about the fabrication and characterization of carbon aerogels in the literature,[1–4] but most carbon aerogel materials were synthesized by the method of carbon dioxide supercritical drying, reported by Pekala.[5] We recently reported a new method for the synthesis of carbon aerogels.[6] In this work, we have synthesized an organic gel from resorcinol and furfural in isopropanol using HCl as a catalyst, and then directly drying the resulting material under isopropanol supercritical conditions, followed by carbonization in a nitrogen atmosphere. This method omits the steps of exchanging water with an organic solvent (acetone) and an organic for carbon dioxide before supercritical drying, so that the new method is a simpler, easier, and safer process than the typical method of carbon dioxide supercritical drying commonly used at present. In the previous work,[6] we reported the fabrication conditions and the properties characterization of the carbon aerogels thus produced. In this paper, we focus on studies of the chemical structure and especially the pore structure of the carbon aerogels obtained, because the pore structure greatly affects the adsorption and other properties of the aerogels. Thus, by using X-ray photoelectron spectroscopy (XPS), scanning electron microscopy (SEM), and a surface area analyzer, the chemical states of carbon and oxygen, the morphology, and the pore parameters and pore distributions within the samples were investigated. This work thus provides detailed information on the effect of modification of the fabrication procedures on the

Correspondence to: M. S. Dresselhaus (millie@mgm.mit.edu).

Contract grant sponsor: Lawrence Livermore National Laboratory; subcontract grant number: B518047.
Contract grant sponsor: National Natural Science Foundation of China; contract grant number: 59973028.
Contract grant sponsor: Talents Training Program Foundation of the Higher Education Department of Guangdong Province.
Contract grant sponsor: NASA; contract grant number: NAG-1–01,061 through a subcontract from UNC.

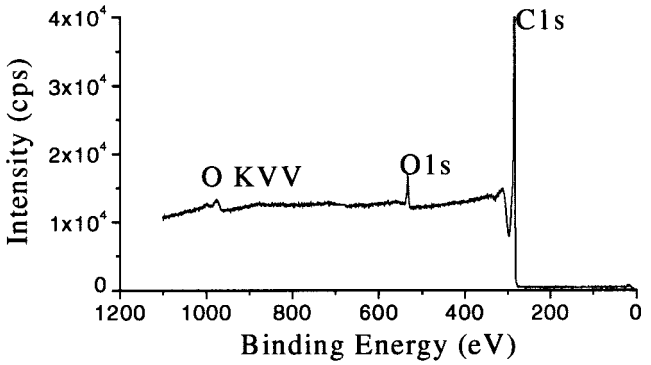

Figure 1 XPS spectrum of CA-IPA CA-59.

properties of the carbon aerogels and on the selection of materials for specific uses.

EXPERIMENTAL

Sample preparation

The preparation of carbon aerogels has been previously reported.[6] The synthesis involves the gel polymerization of resorcinol with furfural in isopropanol using HCl as a catalyst, and then drying the resulting material directly under isopropanol supercritical conditions, followed by carbonization at 800°C under a nitrogen atmosphere. The samples thus produced were denoted by CA-IPA.

XPS determination

XPS characterization of the carbon aerogels was carried out on an AXIS HIS 165 and ULTRA Spectrometer made by Kratos Analytical Ltd. England, using Al K_α radiation (energy 1,486.6 eV) in a vacuum of 5×10^{-9} Torr. X-ray slots of 760×350 μm^2 and an X-ray power of 150 W (15 kV and 10 mA) were used for all of the XPS measurements.

TABLE I
Elemental Contents of the CA-IPA Samples

	Sample no.		
	CA-57	CA-59	CA-60
Mass density (mg/ml)	479	424	231
Carbon			
Atomic content (%)	97.31	97.06	97.94
Mass content (%)	96.44	96.12	97.27
Oxygen			
Atomic content (%)	2.69	2.94	2.06
Mass content (%)	3.56	3.88	2.73

SEM observation

The samples were mounted on a sample holder with silver paint and coated with an Au/Pd alloy. The morphology images of the samples were recorded using a JEM-6320FV scanning electron microscope.

Measurement of pore parameters and pore size distribution

Samples of approximately 0.1 g were heated to 200°C to remove all the adsorbed species. Nitrogen adsorption isotherms were then taken using an ASAP 2000 surface area analyzer (Micromeritics Instrument Corp.). The Horvath—Kawazoe (HK) and Barrett—Joyner—Halendar (BJH) theories were used for the analysis of the micropore and mesopore distribution, respectively.

RESULTS AND DISCUSSION

Chemical structure of the CA-IPA samples

Figure 1 is an XPS survey scan of a typical CA-IPA. The result indicates that the CA-IPA sample mainly consists of the elements carbon and oxygen (the element hydrogen can not be detected by XPS). The content of chloride (from the HCl catalyst) is too low to be seen in the CA-IPA spectrum that was obtained. According to the survey scan, the elemental contents of the CA-IPA samples are listed in Table I. We can see that all of the CA-IPA samples have similar elemental content. They have higher carbon content and lower oxygen content than that of the potassium-containing carbon aerogels and of the copper-doped carbon aerogels reported in previous work.[7] The detailed scanning of C1s and O1s (see Figs. 2 and 3) shows that the C1s and O1s spectra of the CA-IPA samples prepared under different conditions are almost the same, indi-

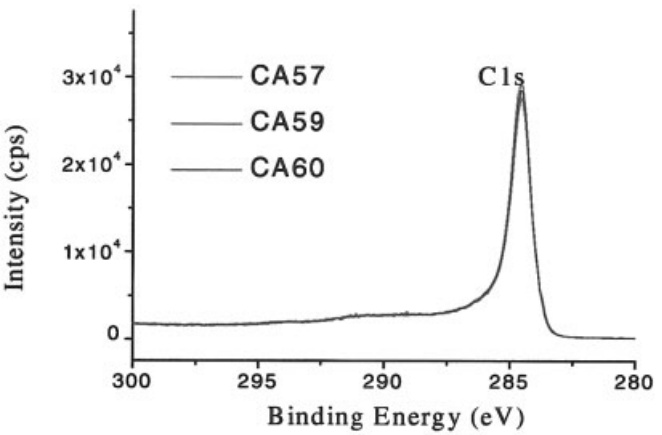

Figure 2 The C1s spectra of the CA-IPA samples.

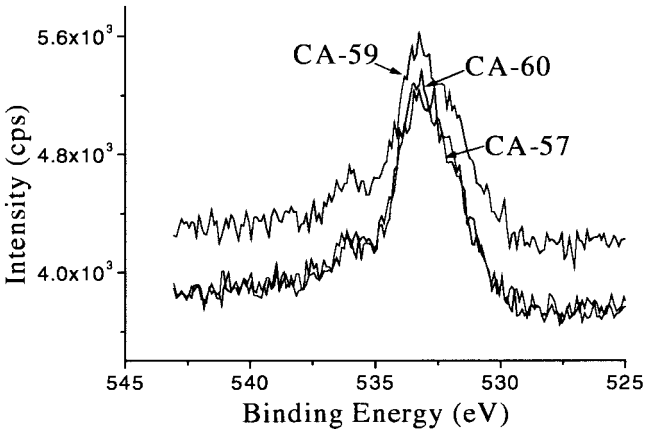

Figure 3 The O1s spectra of the CA-IPA samples.

cating that the CA-IPA samples have almost the same chemical structure, even though they possess different morphology and pore structures as discussed below.

It can be seen from Figure 2 that the C1s peaks of all CA-IPA samples are very sharp. The values of their full widths of half maximum (FWHM) intensity are only about 0.97 eV. However, their C1s spectra are also asymmetric and tail toward high binding energies, suggesting that the CA-IPA samples still contain a small amount of oxygen-containing surface groups.

According to previous studies in the literature,[8–13] a C1s curve fitting technique is usually used for the analysis of oxygen-containing surface groups on carbon materials. Referring to the literature,[8–13] we assigned the main peak at about 284.5 eV to aromatic and aliphatic carbon, the peak at about 285.9 eV to a hydroxyl group, the peak at about 287.6 eV to a carbonyl group, the peak at about 289.1 eV to the carboxyl group, and the peak at about 290.8 eV to the shake-up satellite, and we then performed the curve fitting of the C1s spectra of the CA-IPA samples. We were unable to obtain good results when we first tried to fit the C1s spectra by assuming the component peaks to be of the Gaussian type, as commonly used. However, when we chose the peak type to be a Gaussian–Lorentzian Cross Product, we obtained very good curve fitting results, which are shown in Figures 4(a) to 4(c). The curve fitting data are listed in Table II.

It can be seen from Table II that there are about 30% oxygen-containing surface groups on the CA-IPA samples. Among them, most are hydroxyl groups (about 17%). The contents of the carbonyl and the carboxyl groups are approximately 7 and 5.5%, respectively. The type and amount of the oxygen-containing groups in the various CA-IPA samples are similar.

We also performed curve fitting of the O1s feature for the CA-IPA samples [see Fig. 5(a) to 5(c)] by assigning the peak at about 533.2 eV to single bond

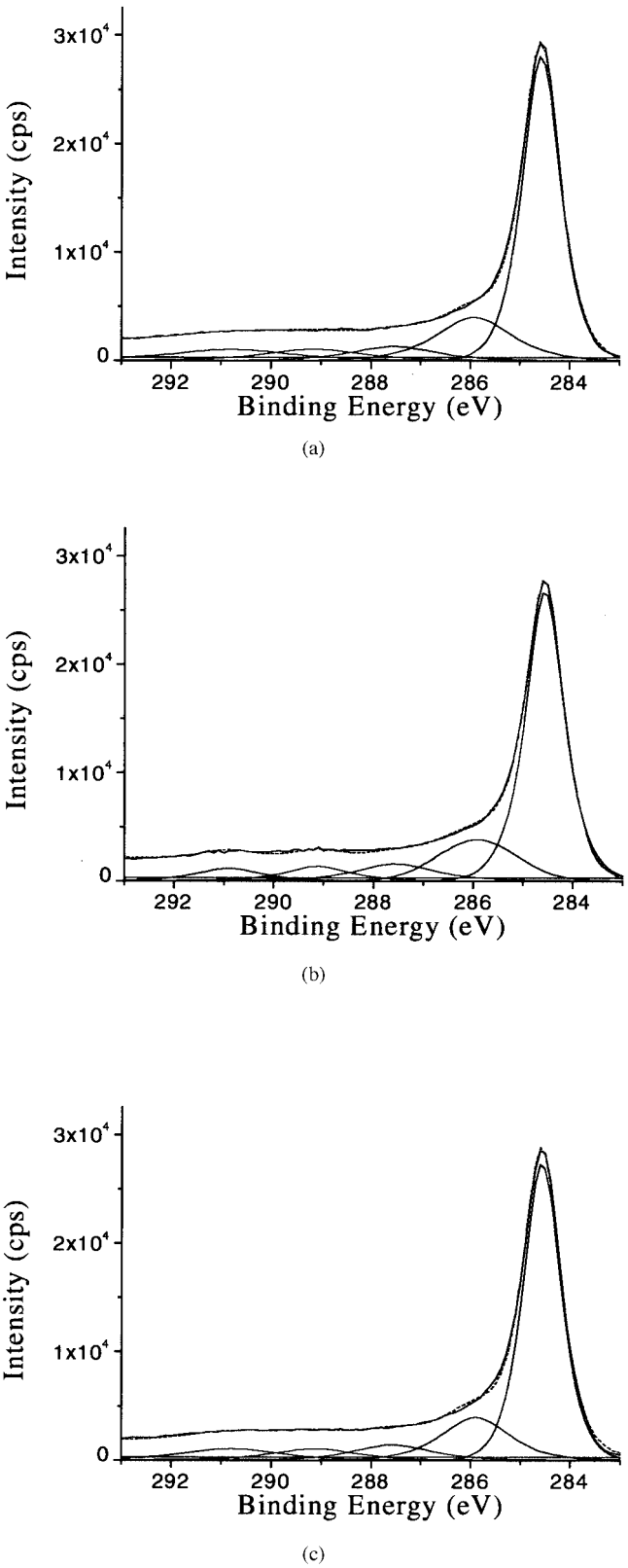

Figure 4 (a) Curve fitting result of C1s of CA-IPA CA-57. (b) Curve fitting result of C1s of CA-IPA CA-59. (c) Curve fitting result of C1s of CA-IPA CA-60.

TABLE II
Curve Fitting Data of the C1s Spectra of the CA-IPA Samples

Sample no.	Component peak	Position BE* (eV)	FWHM* (eV)	Raw area (cps)	Area (%)
	1	284.58	0.898	29200.35	63.12
	2	285.93	1.780	8209.76	17.75
CA-57	3	287.53	1.993	2987.36	6.46
	4	289.14	1.933	2770.54	5.99
	5	290.80	2.533	3094.24	6.69
	1	284.56	0.907	28508.22	65.15
	2	285.92	1.875	7596.28	17.35
CA-59	3	287.56	1.842	3367.31	7.69
	4	289.12	1.681	2335.40	5.34
	5	290.90	2.126	1953.95	4.47
	1	284.56	0.889	27916.98	64.82
	2	285.90	1.607	7272.39	16.89
CA-60	3	287.57	1.819	2940.11	6.83
	4	289.14	1.942	2314.67	5.37
	5	290.80	2.260	2621.25	6.09

*BE, binding energy; FWHM, full width half maximum intensity linewidth.

oxygen and the peak at about 531.7 eV to double bond oxygen.[8–10] The curve fitting data are listed in Table III. We can see that most of the oxygen element (~68%) is in the chemical state of single bond oxygen.

Morphology of the CA-IPA

Though we have analyzed the carbon framework of the nanostructure of the CA-IPA samples by transmission electron microscopy observations, and we have found that the CA-IPA samples consist of interconnected carbon nanoparticles,[6] the SEM observation can give us some detailed information about the morphology and texture, especially the mesopore and macropore structure of the CA-IPA. Figures 6(a) to 6(h) show SEM photographs of several CA-IPA samples with various mass densities. It can be seen that the carbon nanoparticles are packed into a network in the CA-IPA. There are many mesopores and macropores among the carbon nanoparticles. The size and the shape of individual carbon nanoparticles observed in different samples are almost the same, but the packing space is greatly changed with the change of mass density of the CA-IPA. We find from Figures 6(a) to 6(h) that when the density of the CA-IPA decreases, the number of macropores with sizes over several hundred nanometers increases. Therefore, we can control the mesopore and macropore structures by controlling the mass density of CA-IPA through changing the mass content of the reactants.

Because the change of mass density mainly changes the number of mesopores and especially the number of macropores, but the individual carbon nanopar-

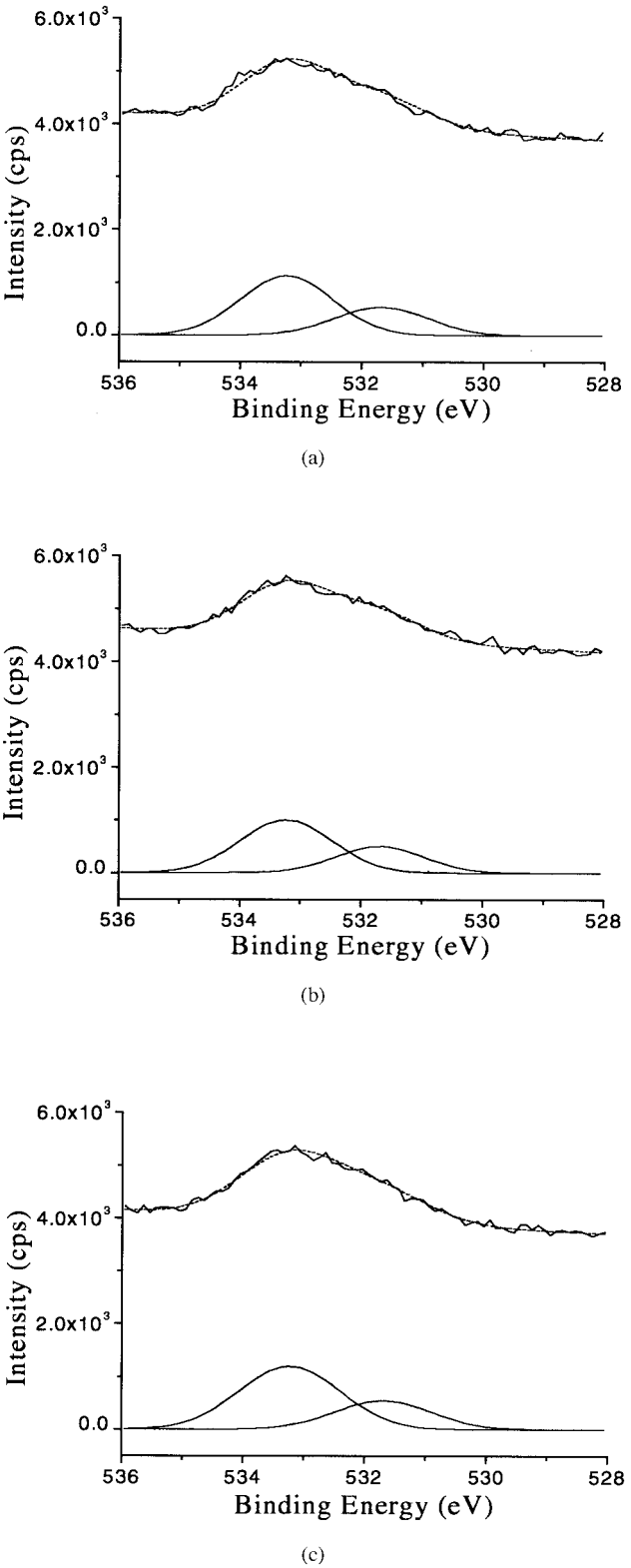

Figure 5 (a) Curve fitting result of O1s of CA-IPA CA-57. (b) Curve fitting result of C1s of CA-IPA CA-60. (c) Curve fitting result of C1s of CA-IPA CA-59.

TABLE III
Curve Fitting Data of the O1s Spectra of the CA-IPA Samples

Sample no.	Component peak	Position BE* (eV)	FWHM* (eV)	Raw area (cps)	Area (%)
CA-57	1	531.68	1.804	1025.46	32.42
	2	533.24	1.786	2137.96	67.58
CA-59	1	531.69	1.875	1088.67	30.40
	2	533.23	1.962	2492.01	69.60
CA-60	1	531.69	1.703	906.96	32.23
	2	533.23	1.789	1907.35	67.77

*BE, binding energy; FWHM, full width half maximum intensity linewidth.

ticles are kept the same, the surface area of the CA-IPA increases only slightly when the mass density greatly decreases.[6]

Pore parameters and pore size distribution of the CA-IPA

The SEM observations indeed demonstrate the effect of the mass density on the mesopore and macropore structures of CA-IPA, but give no quantitative information. Here, we mainly focus on the relationship between the mass density and the pore structures. The characterization of pore parameters and pore size distribution will provide quantitative and detailed information of the pore structure of the CA-IPA samples.

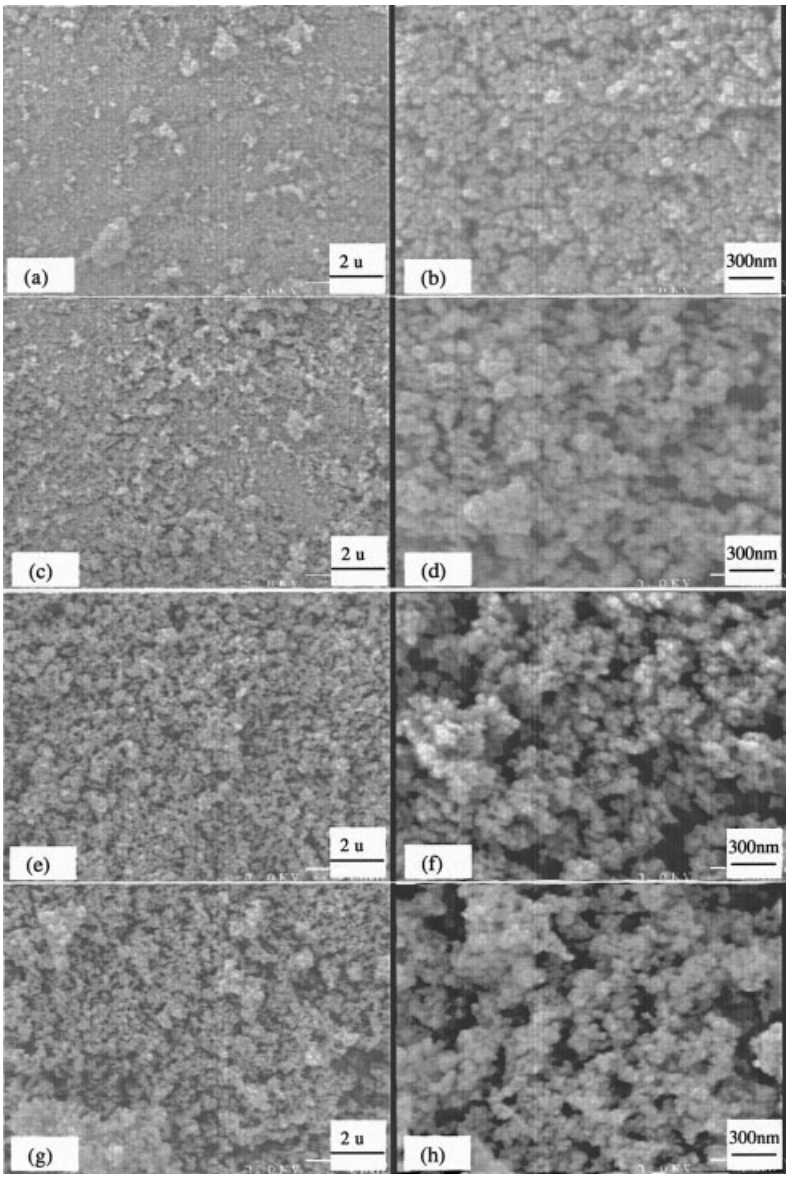

Figure 6 SEM photographs of the CA-IPA samples with various mass densities (a and b) 479 mg/ml; (c and d) 424 mg/ml; (e and f) 231 mg/ml; (g and h) 148 mg/ml.

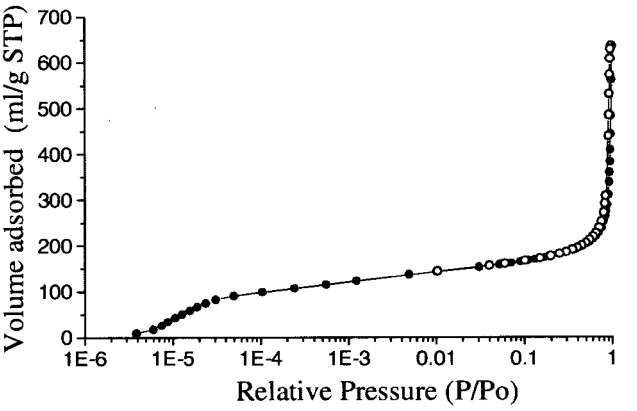

(a)

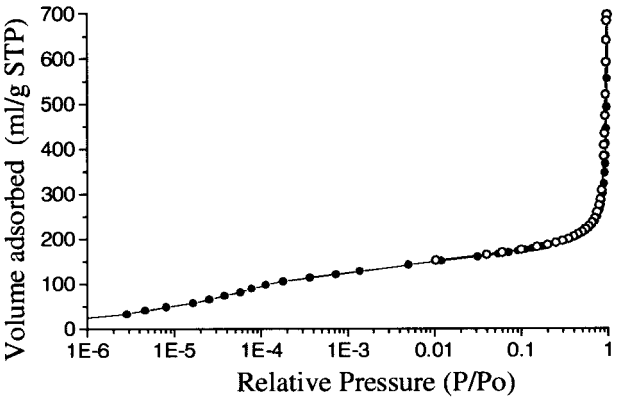

(b)

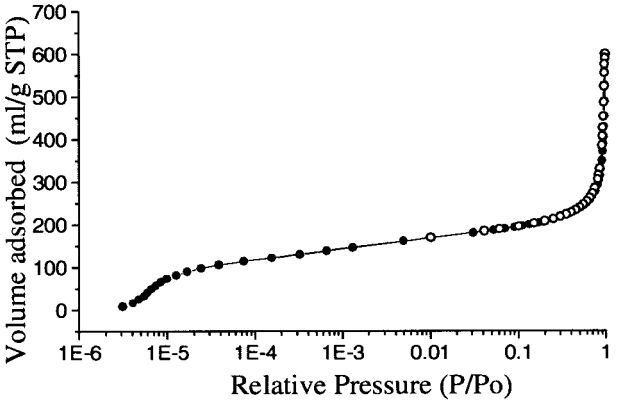

(c)

Figure 7 (a) The isotherm of the CA-IPA CA-57. (b) The isotherm of the CA-IPA CA-62. (c) The isotherm of the CA-IPA CA-63.

Figures 7(a) to 7(c) show the adsorption–desorption isotherms of the samples of various densities. All the samples were found to give type IIb nitrogen isotherms.[14] The isotherms in Figure 7 rise very sharply at low relative pressures and reach a high adsorption volume, indicating that the CA-IPA samples contain a large amount of micropores. With increasing relative pressure, the isotherms become almost linear. At high relative pressure, the isotherms exhibit a hysteresis loop.

According to the isotherms of the CA-IPA samples, the surface area, pore volume, and pore size of the CA-IPA samples are listed in Table IV. We can see that for the CA-IPA samples prepared at the same temperature, the micropore volume of the samples increases with a decrease in the mass density. The alternative tendency of the micropore volume and the Brunauer—Emmett—Teller (BET) surface area of the CA-IPA samples to increase with decreasing mass density are almost the same. However, all of the mesopore volume (BJH desorption cumulative pore volume between 1.7 and 300 nm diameter), the single point total pore volume (at $P/Po = 0.98$), the median pore diameter, the BJH desorption average pore diameter (4V/A), as well as the average pore diameter (4V/A by BET) of the CA-IPA samples have a maximum value with a decrease of its mass density. We explain these results as follows.

The mesopores in the CA-IPA are attributed to the interval gaps between the carbon nanoparticles. For the high mass density CA-IPA samples, the carbon nanoparticles are packed tightly and have a small amount of interval gaps. Therefore, its mesopore volume and single point total pore volume are lower and its median pore diameter, BJH desorption average pore diameter (4V/A), and average pore diameter (4V/A by BET) are all small. When the mass density of the CA-IPA decreases, the number and size of the interval gaps between the carbon nanoparticles increase, therefore, the mesopore volume and relative pore diameter in Table IV increase. However, when the mass density of the CA-IPA decreases too much, many mesopores will be enlarged into macropores that cannot be detected by the ASPA 2000 Surface Area Analyzer, as observed in the SEM study above. Therefore, the mesopore volume, single point pore volume, and relative pore diameter in Table IV decrease.

We analyzed the micropore distribution of the CA-IPA samples by the HK method[14] and the results are shown in Figure 8. It can be seen that all of the CA-IPA samples with various mass densities have very narrow micropore size distributions and most micropores are concentrated at a diameter of about 0.5 nm.

We assessed the mesopore distribution of the CA-IPA samples by the BJH method[14] and the results are shown in Figure 9. We can see from Figure 9 that the mesopore size distribution of the CA-IPA is widened and the peak value of distribution curve is shifted to

TABLE IV
Surface Area, Pore Volume, and Pore Diameter of the CA-IPA Samples*

	Sample No.				
	CA-59#	CA-60#	CA-57#	CA-62#	CA-63#
Gelation temperature (°C)	60	60	70	70	70
Mass content of reactants (wt %)	11.5	5.9	16.7	11.5	5.9
Mass density of carbon aerogel (mg/ml)	424	231	479	323	148
BET surface area (m^2/g)	615.3	630.4	557.1	583.5	655.6
Micropore volume (ml/g)	0.186	0.189	0.171	0.177	0.202
BJH desorption cumulative pore volume (ml/g)	1.093	0.810	0.842	0.918	0.744
Single point total pore volume (ml/g)	1.253	0.979	0.981	1.075	0.926
Median pore diameter (nm)	46.2	21.8	30.9	37.4	15.7
BJH desorption average pore diameter (4V/A) (nm)	15.1	11.0	12.2	13.5	10.1
Average pore diameter (4V/A by BET) (nm)	8.15	6.21	7.05	7.37	5.65

*BET, Brunauer-Emmett-Teller; BJH, Barrett-Joyner-Halendar.

higher diameters as the mass density of the CA-IPA decreases. These changes are caused by the size increase of many of the mesopores in the CA-IPA and finally by their transition into macropores, consistent with the SEM observation results mentioned above.

CONCLUSION

The CA-IPA samples produced by the gelation and supercritical drying in isopropanol have a high carbon content and a low oxygen content. The content of chloride is too low to be detected by XPS. The chemical structures of the CA-IPA samples produced in our experiments are almost the same. The oxygen-containing groups on the surface of the CA-IPA can be assessed by the curve fitting of its C1s spectrum by assuming the component peak type to be a Gaussian–Lorentzian Cross Product.

The size and shape of the individual carbon nanoparticles in various CA-IPA samples are almost the same, but their packing space varies highly. When the density of the CA-IPA decreases, the macropores with sizes over several hundred nanometers apparently increase.

The micropore volume of the CA-IPA increases with a decrease in the mass density, but the mesopore volume, the single point total pore volume, the median pore diameter, the BJH desorption average pore diameter, and the average pore diameter of the CA-IPA samples have a maximum value at a certain mass density. The CA-IPA samples have a very narrow micropore distribution at about 5 nm. The mesopore size distribution of the CA-IPA is widened and the peak value of the distribution curve is shifted to higher diameters as the mass density of the CA-IPA decreases.

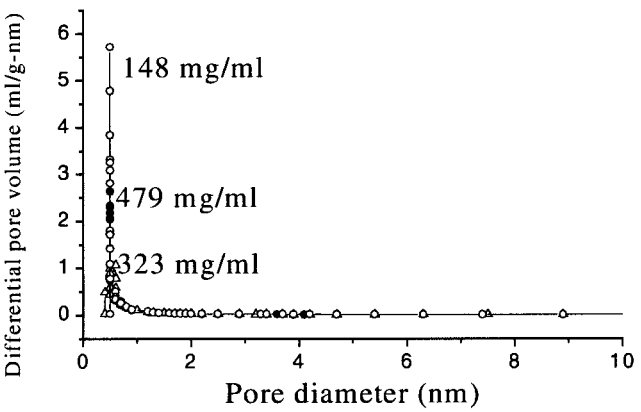

Figure 8 Micropore distribution of the CA-IPA samples.

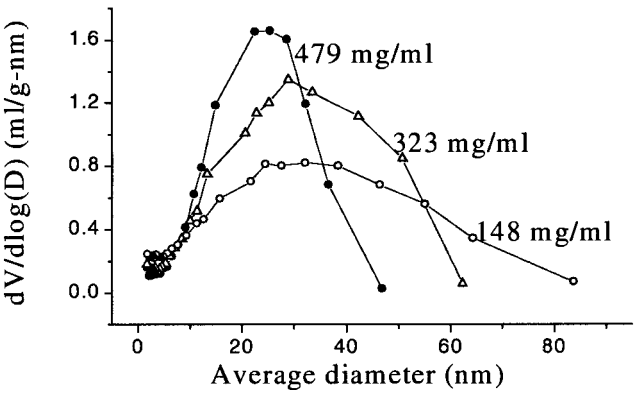

Figure 9 Mesopore distribution of the CA-IPA samples with different mass densities.

The research at MIT was supported by Lawrence Livermore National Laboratory Subcontract B518047 and partially supported by the National Natural Science Foundation of China (59973028) and by the Talents Training Program Foundation of the Higher Education Department of Guangdong Province. Work at Duke University is in part supported by a grant from NASA (NAG-1–01,061) through a subcontract from UNC.

References

1. Dresselhaus, M. S.; Dresselhaus, G; Eklund, P. C. Science of Fullerenes and Carbon Nanotubes; Academic: New York, 1995.
2. Smith, D. M.; Stein, D.; Anderson, J. M.; Ackerman, W. J Non-Cryst. Solids 1995, 186, 104.

3. Desphande, R.; Smith, D. M.; Brinker, C. J. US Patent 5565142, 1996.
4. Pekala, R. W.; Alviso, C. T.; Lu, X.; Gross, C. J; Fricke, J. J Non-Cryst. Solids 1995, 188, 34.
5. Pekala, R. W. US Patent 4 873 218, 1989.
6. Fu, R.; Zheng, B.; Liu, J.; Dresselhaus, M. S.; Dresselhaus, G.; Satcher, J.; Baumann, T. J Mater Res 2003, 18, 2765.
7. Yoshizawa, N.; Fu, R.; Dresselhaus, M. S.; Dresselhaus, G.; Satcher, J.; Baumann, T. Proceedings of MRS Fall Meeting, Boston; November 2001.
8. Wang, D.-B.; Chen, B.-H.; Zhang, B.; Ma, Y.-X. Polyhedron 1997, 16, 2625.
9. Fu, R.; Zeng, H. Synth Fiber Ind (in Chinese) 1990, 13, 19.
10. Cuesta, A.; Martinez-Alonso, A.; Tascon, J. M.; Bradley, R. H. Carbon 1997, 35, 967.
11. Figueiredo, J. L.; Pereira, M. F. R.; Freitas, M. M. A.; Orfao, J. J. M. Carbon 1999, 37, 1379.
12. Polovina, M.; Babic, B.; Kaluderovic, B.; Dekanski, A. Carbon 1997, 35, 1047.
13. Moreno-Castilla, C.; Lopez-Ramon, M. V.; Carrasco-Marin, F. Carbon 1995, 38, 2000.
14. Rouquerol, F.; Rouquerol, J.; Sing, K. Adsorption by Powders and Porous Solids, Principles, Methodology and Applications; Academic: New York, 1999.